

Nonlinear Response of a Quantum System to Impulsive Perturbations: A Non-Perturbative Real-Time Approach

Alberto Guandalini,^{*,†,‡} Caterina Cocchi,^{¶,§} Stefano Pittalis,[‡] Alice Ruini,^{†,‡} and Carlo A. Rozzi^{*,‡}

[†]*Dipartimento di Scienze Fisiche, Informatiche e Matematiche, Università di Modena e Reggio Emilia, Via Campi 213A, I-41125 Modena, Italy*

[‡]*CNR – Istituto Nanoscienze, Via Campi 213A, I-41125 Modena, Italy*

[¶]*Physics Department and IRIS Adlershof, Humboldt-Universität zu Berlin, Zum Großen Windkanal 6, D-12489 Berlin, Germany*

[§]*Carl von Ossietzky Universität Oldenburg, Physics Department, D-26129 Oldenburg, Germany*

E-mail: alberto.guandalini@unimore.it; carloandrea.rozzi@nano.cnr.it

Abstract

We argue that real-time propagation of quantum states as induced by instantaneous electrical impulses can be an ideal computational tool for investigating nonlinear optical properties of many-electron systems especially when, as in the case of optical limiting, the relevant nonlinearities are not restricted to wave mixing at a predefined order. We demonstrate the capabilities of this methodology through an application to a one-dimensional model system. We show that the Fourier transform of the computed non-linear cross section describes excited state absorption at all resonances *and* all orders, also in case of slow convergence of the perturbative series.

1 Introduction

Nonlinear optics globally refers to the regime in which the polarization induced in a material by an electric field is not directly proportional to the magnitude of the external field. All optical media are intrinsically nonlinear, but it is only with the development of high power lasers, that nonlinear properties have become accessible and hence extensively studied.¹⁻³

The standard theoretical approach to nonlinear optics rests on perturbation theory, in which the polarization induced in a quantum system by a (classical) electric field is expressed as a power series in the field strength.⁴ Full rigor would require that the power series converges, but one is usually interested in the susceptibilities calculated at a some finite n th-order. The development of femtosecond and attosecond lasers has pushed the largest available peak intensity toward magnitudes of the electric field comparable with or larger than those experienced by electrons in the atoms.⁵ These light sources have thus provided direct access to a variety of resonant regimes in which perturbation theory is not suitable:⁶ To explore the corresponding phenomenology⁷⁻⁹ a non-perturbative solution is in order.

Direct numerical time propagation of a quantum state subject to time-dependent fields provides us with a numerical approach that, in principle, does not suffer from the limitation of perturbative series expansions.¹⁰ First-principles frameworks such as time-dependent density functional theory (TDDFT)^{11,12} enable realistic simulations of both steady-state and time-resolved spectroscopies for large systems that cannot be tackled by means of more accurate but also more computationally demanding methods.¹³⁻¹⁶ The linear and non-linear regimes can, in principle, be tackled on equal footings within the same framework. Moreover, the inclusion of nuclear dynamics is straightforward.¹⁷⁻²¹ Extensions for describing the propagation in presence of decoherence, dissipative environments, or coupling to other external degrees of freedom, are also available.²²

When applied to compute the linear-response of a system, the time-propagation

method is often formulated in terms of impulse response theory. In such a case, for time-invariant dynamical systems, the impulse response to an external perturbation is a property of the unperturbed system and is independent of the specific temporal shape of the perturbation: Given the knowledge of the impulse response alone, it is possible to predict the response to any small perturbation by means of the convolution theorem.²³ However, this procedure is not applicable as non-linear effects become important. Yet, in some important cases, the dependence of the response on the external field may be relatively simple.

As a primary example, a version of the impulse response method in the time domain was recently applied²⁴ to the description of optical limiting due to reverse saturable absorption.^{25,26} The method was found to be capable of providing a good description of the main spectral features, including the appearance of new absorption bands above a threshold value of the incoming light intensity. The simplicity of the non-linear process that drives the reverse saturable absorption may justify the success of the aforementioned approach: The threshold mechanism corresponds to the activation of an excited-state absorption channel, when the intensity of the incoming light allows for sufficient population of the excited state itself.^{27,28} As long as the steady-state absorption is observed by means of continuous wave lasers (*i.e.*, we are only concerned with a time-invariant observable) the spectrum depends on the intensity, but not on the detailed shape or phase of the impinging light.

Although there are cases, such the one mentioned above, where the calculated impulsive response may be related to the observed nonlinear absorption, to the best of our knowledge, a thorough examination of the effects of an impulsive initial perturbation has not yet been reported in the nonlinear regime. To fill this gap, after some preliminary analytic work, we study herein the response of an exactly solvable one-dimensional (1D) system acted upon an impulsive electrical field. We critically discuss the resulting field-dependent absorption spectra by identifying the transitions and the excited states involved in the process and we compare results with those given by standard perturbation theory.

This work is organized as follows: In Section 2 the expression of the absorption cross section and its spectral resolution is derived for an instantaneous impulsive exciting field of arbitrary strength within the dipole approximation. The cross section is analyzed both in the nonlinear case and in the weak field limit. The complementarity of the proposed methodology and regular perturbative theory is discussed. In Section 3 the linear and nonlinear absorption of two electrons in a 1D infinite well is simulated by means of a numerical time-propagation scheme. The absorption cross section is interpreted by means of the previously derived expressions, distinguishing the contribution of ground-state and excited-state absorption at different field strengths. Finally, the validity, the usefulness, and the limitations of the proposed methodology to simulate nonlinear properties in complex materials are discussed.

2 Absorption Cross Section in the instantaneous Impulsive Limit

Let us consider a system of N interacting electrons subject to a time-dependent classical electric field in the dipole approximation described by the Hamiltonian $\hat{H}(t) = \hat{H}_0 - \hat{d}_\mu \mathcal{E}_\mu(t)$ (summation over repeated indices is understood), where H_0 includes the ordinary electron-nuclei and electron-electron Coulomb interaction, $\hat{d}_\mu = \sum_{i=1}^N \hat{r}_\mu^i$ is the electric dipole operator with \hat{r}_μ^i , and $\mu = x, y, z$ is the μ -th component of the position operator of the i -th electron. Spin-orbit coupling is neglected. We aim to describe the light absorption process in the case of an extremely short pulse, *i.e.* in the limit of a Dirac delta time-dependence

$$\mathcal{E}_\mu(t) = \kappa_\mu \delta(t). \quad (1)$$

We make no particular assumptions about the value of $\kappa \equiv \sqrt{\kappa_\mu \kappa_\mu}$. Here, we focus our analysis on absorption at equilibrium, *i.e.* we suppose that the system is in its ground state for $t < 0$, namely $|\Psi(t < 0)\rangle = |\Psi_0\rangle e^{-iE_0 t}$. For a description of the out-of-equilibrium absorption processes, as in the case of time-resolved absorption

spectroscopy, further analysis is required.²⁹

For $t > 0$, the solution of the time-dependent Schrödinger equation $|\Psi(t)\rangle$ can be projected on the eigenstates $\{|\Psi_i\rangle\}$ of \hat{H}_0 as

$$|\Psi(t > 0)\rangle = \sum_{i=0}^{+\infty} c_i |\Psi_i\rangle e^{-iE_i t}, \quad (2)$$

where $\{E_i\}$ are the eigenvalues of \hat{H}_0 . The coefficients c_i are

$$c_i = \langle \Psi_i | e^{-i\hat{d}_\mu \kappa_\mu} | \Psi_0 \rangle. \quad (3)$$

Due to the instantaneous nature of the perturbation, the c_i coefficients are time-independent. The time-dependent dipole moment $d_\mu(t) = \langle \Psi(t) | \hat{d}_\mu | \Psi(t) \rangle$ for such a system is

$$d_\mu(t) = \theta(t) \sum_{i,j=0}^{+\infty} c_i^* c_j d_\mu^{ij} e^{-i\omega_{ji}t} + \theta(-t) d_\mu^{00}, \quad (4)$$

where $\theta(t)$ is the Heaviside theta function, $d_\mu^{ij} = \langle \Psi_i | \hat{d}_\mu | \Psi_j \rangle$ are the dipole matrix elements, d_μ^{00} is the ground state dipole, and $\omega_{ji} = E_j - E_i$.

We wish now to employ the explicit shape for the dipole moment in Eq. (4) in order to calculate the absorption cross section

$$\sigma(\omega) = \frac{4\pi\omega}{c} \frac{\text{Im} [d_\mu(\omega) \mathcal{E}_\mu^*(\omega)]}{|\mathcal{E}(\omega)|^2}. \quad (5)$$

The full derivation of Eq. (5) is provided in the Supplementary Infomation, showing that this expression is not limited to the weak field regime.

By Fourier transforming Eq. (4), substituting it into Eq. (5), and assuming, for sake of simplicity, that the system is centrosymmetric (*i.e.* $d_\mu^{00} = 0$), we obtain

$$\sigma(\omega) = \frac{4\pi^2}{c\kappa^2} \sum_{i,j>i} [C_{0i}S_{j0} - S_{0i}C_{j0}] M_{ij}\omega_{ji}\delta(\omega_{ji} - \omega), \quad (6)$$

where $C_{ij} \equiv \langle \Psi_i | \cos(\hat{d}_\mu \kappa_\mu) | \Psi_j \rangle$, $S_{ij} \equiv \langle \Psi_i | \sin(\hat{d}_\mu \kappa_\mu) | \Psi_j \rangle$, and $M_{ij}^{(n)} \equiv$

$\langle \Psi_i | (\hat{d}_\mu \kappa_\mu)^n | \Psi_j \rangle$ with $M_{ij}^{(1)} \equiv M_{ij}$. Eq. (6), derived in the Supplementary Information, can be used to describe, for example, an ensemble of molecules (*e.g.*, in the gas phase) randomly oriented with respect to the electric-field direction. Since the ensemble-averaged optical response is centrosymmetric regardless of the point symmetry of the individual molecules, the average cross section is obtained by sampling and averaging the responses to impulses with different polarization directions.

In order to highlight the nonlinear character of the cross section, we compute the linear absorption cross section $\sigma^{(1)}(\omega)$ by approximating the matrix elements in Eq. (6) up to the first order in κ . Since $\sin(\hat{d}_\mu \kappa_\mu) \approx \hat{d}_\mu \kappa_\mu$ and $\cos(\hat{d}_\mu \kappa_\mu) \approx \hat{1}$, we have

$$\sigma^{(1)}(\omega) = \frac{4\pi^2\omega}{c\kappa^2} \sum_{j=0}^{+\infty} |M_{j0}|^2 \delta(\omega - \omega_{j0}) . \quad (7)$$

Eq. (7) provides a good approximation for Eq. (6) if $\kappa \ll 1/R$, where R is the size of the system. For molecular systems with $R \approx (1-100)$ bohr, a value of $\kappa \approx 10^{-3}$ bohr $^{-1}$ is suitable to define a weak field in the impulsive limit.³⁰

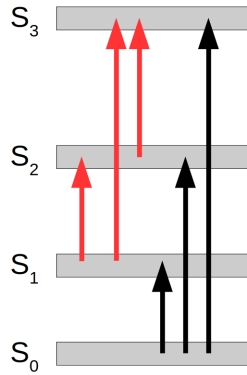


Figure 1: Sketch of ground-state (black) and excited-state (red) excitations in the singlet manifold. Excited-state excitations involve transitions between excited states and are activated in the nonlinear regime described by Eq. (6). Ground-state absorption is described by the ordinary linear cross section in Eq. (7).

While in the linear regime the resonances in the cross section are only found at $\omega = \omega_{j0} \equiv E_j - E_0$, in Eq. (6) the resonances occur at $\omega = \omega_{ji} \equiv E_j - E_i$; *i.e.* for the energy of the incoming light equals the energy difference between any pair of

eigenstates of the unperturbed Hamiltonian \hat{H}_0 . This is sketched in Figure 1, in which black arrows indicate ground-state absorption (GSA) as given by Eq. (7) and red arrows denote excited-state absorption (ESA) as given by Eq. (6). ESA, in practice, can occur when one or more excited states of the unperturbed system are populated by a laser.

Eqs. (6) and (7) share the same dipole parity selection rule, as they include the same matrix elements M_{ij} , with $i = 0$ in Eq. (7). However, while states with the same parity as the ground state cannot be populated in the linear regime, they can be populated in the nonlinear regime through ESA. Observing closely, the individual contributions to Eq. (6) vanish for all the states i with either $C_{0i} = 0$, or $S_{0i} = 0$. In the next section, we exploit this fact to determine the set of transitions that build up the ESA at different field strengths. Also note that, $\sigma(\omega)$ in Eq. (6) satisfies the Thomas–Reiche–Kuhn sum rule in the form

$$\int_0^{+\infty} d\omega \sigma(\omega) = \frac{2\pi^2 N}{c}, \quad (8)$$

where N is the number of electrons. Since the right hand side of Eq. (8) does not depend on κ the sum rule is valid both in the linear and nonlinear regimes.

The perturbative analysis can be carried on by further expanding Eq. (6) in powers of κ . The second order term vanishes because we assumed inversion symmetry. The third order term is

$$\sigma^{(3)}(\omega) = \frac{4\pi^2}{c\kappa^2} \left[\sigma_{\text{GSA}}^{(3)}(\omega) + \sigma_{\text{ESA}}^{(3)}(\omega) \right], \quad (9)$$

where

$$\sigma_{\text{GSA}}^{(3)}(\omega) \equiv -\frac{1}{6} \sum_j \left(M_{0j} M_{j0}^{(3)} + 3M_{00}^{(2)} |M_{j0}|^2 \right) \omega_{j0} \delta(\omega - \omega_{j0}) \quad (10)$$

has poles only at the ground state excitation energies $\omega_{j0} = E_j - E_0$ (see Eq. 7): *i.e.* it describes the third order correction to GSA. Hence, the term

$$\sigma_{\text{ESA}}^{(3)}(\omega) \equiv -\frac{1}{2} \sum_{\substack{i>0 \\ j>i}} \left(M_{0i}^{(2)} M_{j0} - M_{0i} M_{j0}^{(2)} \right) M_{ij} \omega_{ji} \delta(\omega - \omega_{ji}) \quad (11)$$

describes the third order correction to ESA. Note that $\sigma^{(3)}$ includes both excitations and de-excitations from the excited states. The spectral features obtained from the non-linear cross section may therefore have either positive or negative oscillator strengths. Next, the 5th order correction is derived in a similar way as done for the 3rd order

$$\begin{aligned} \sigma^{(5)}(\omega) = & \frac{4\pi^2\omega}{c\kappa^2} \left\{ \frac{1}{120} \sum_j M_{j0}^{(5)} M_{0j}\omega_{j0}\delta(\omega - \omega_{j0}) \right. \\ & + \frac{1}{12} \sum_{i,j>i} \left[M_{0i}^{(2)} M_{j0}^{(3)} - M_{0i}^{(3)} M_{j0}^{(2)} \right] M_{ij}\omega_{ji}\delta(\omega - \omega_{ji}) \\ & \left. + \frac{1}{24} \sum_{i,j>i} \left[M_{0i}^{(4)} M_{j0} - M_{0i} M_{j0}^{(4)} \right] M_{ij}\omega_{ji}\delta(\omega - \omega_{ji}) \right\}. \end{aligned} \quad (12)$$

As observed for $\sigma^{(3)}$, although not shown here explicitly, $\sigma^{(5)}$ can be split into purely GSA and ESA contributions. We will make use of Eq. (12) in the next section.

Alternatively, $\sigma^{(n)}(\omega)$ can be expressed in terms of the n -th order response function.³¹ For example, $\sigma^{(3)}(\omega)$ can be expressed in terms of the third order hyperpolarizability $\gamma_{\alpha\beta\gamma\delta}$ as

$$\sigma^{(3)}(\omega) = \frac{4\pi\omega}{c\kappa^2} \iiint d\omega_1 d\omega_2 d\omega_3 \kappa_\alpha \kappa_\beta \kappa_\gamma \kappa_\delta \text{Im} [\gamma_{\alpha\beta\gamma\delta}(\omega; \omega_1, \omega_2, \omega_3)] \delta(\omega - \omega_1 - \omega_2 - \omega_3). \quad (13)$$

$\gamma_{\alpha\beta\gamma\delta}$ in Eq. (13) allows us to address wave mixing at the third order. In particular, any two-photon absorption process at ω can be captured through $\gamma_{\alpha\alpha\beta\beta}(\omega; \omega, -\omega, -\omega)$.

Even if Eq. (9) also includes two-photon processes, the impulsive field has a fixed frequency dependence. Therefore it cannot predict spectra obtained by means of non-impulsive field shapes. On the other hand Eq. (9) allows us to directly identify the spectral weight due to specific set of transitions at a common resonance. Consequently, accessing $\sigma(\omega)$ with an instantaneous impulse is most useful to describe ESA (which is fluence dependent) but it is not suitable for a full description of two-photon absorption (which is irradiance dependent).³²

Obviously, the impulse response obtained from real-time propagation of the quantum state is intrinsically non perturbative: namely, from the evolved quantum state

we compute $d_\mu(t) = \langle \Psi(t) | \hat{d}_\mu | \Psi(t) \rangle$ and, thus, the Fourier transform $d_\mu(\omega)$ can be readily obtained. The latter finally can be used in (5). According to the previous analysis, the approach captures ESA at *all* the possible resonances.

Furthermore, in practice, we may not need to propagate the quantum state itself. Because $d_\mu(t)$ can be expressed in terms of the particle density explicitly, $d_\mu(t) = \int d^3r r_\mu n(\mathbf{r}, t)$, the procedure based on real-time propagation can be readily implemented in any code that solves the time-dependent Kohn-Sham equations. Thus, large systems can be tackled efficiently within TDDFT approximations.²⁴

Before moving on to discuss an application to gain further insights, we emphasize that, spin-orbit coupling and magnetic fields are not included in our considerations. We work under the assumption that the ground state is a spin singlet, thus, both the expressions in Eq. (6) and Eq. (7) allow transitions only within the manifold of *singlet* excited states. Studying the absorption of excited states with different spin multiplicity is important, for example, to account for inter-system crossing³³ which can occur in optical limiting processes. Formally, this would require to use spin-dependent impulses.³⁴

3 Analysis of Nonlinear Absorption in a 1D Model System

Here we provide a case study of the information that can be extracted by means of the real-time propagation induced by an initial impulsive field. After characterizing the ground-state properties, we calculate the response of a model system for several values of the impulsive field by numerically solving the time-dependent Schrödinger equation. Thus, in light of the expressions derived in the previous Section, we analyze the absorption cross sections in detail.

The considered system consists of two interacting electrons confined in a one-dimensional segment by a potential well of infinite depth (hereafter 1DW). The unper-

turbed Hamiltonian of the 1DW is

$$\hat{H}_0 = \sum_{i=1}^2 \left[-\frac{1}{2} \frac{\partial^2}{\partial x_i^2} + v_{ext}(x_i) \right] + \frac{1}{\sqrt{1 + (x_1 - x_2)^2}}, \quad (14)$$

with the external potential

$$v_{ext}(x_i) = \begin{cases} 0 & -L/2 < x_i < L/2 \\ \infty & \text{otherwise} \end{cases}. \quad (15)$$

The second term in Eq. (14) is the Coulomb interaction between the two electrons, which is softened to avoid the singularity at $x_1 = x_2$.³⁵ For the numerical simulation we have employed the Octopus code.^{36,37} \hat{H}_0 is symmetric under particle interchange $x_1 \leftrightarrow x_2$. Hence, we can choose the spatial component of the wavefunction to be either symmetric or antisymmetric with respect to the exchange of the spatial coordinates. The eigenstates belong to the irreducible representation of either singlet or triplet spin multiplicity. In addition, \hat{H}_0 has also spatial inversion symmetry. Consequently, the orbital part of the wavefunctions must be either even or odd under inversion of the coordinates.

The time-dependent polarization is calculated as $d(t) = \langle \Psi(t) | \hat{d} | \Psi(t) \rangle$ and its Fourier transform $\tilde{d}(\omega)$ enters the absorption cross section

$$\sigma(\omega) = \frac{4\pi\omega}{c} \frac{\text{Im}[\tilde{d}(\omega)]}{\kappa}. \quad (16)$$

The eigenstates and eigenfunctions of this system are shown in Figure 2. The singlet and triplet states are labeled as S_i and T_i , respectively, where the subscript i labels the ground state ($i = 0$) and the excited states. The superscripts g (*gerade*) and u (*ungerade*) indicate the parity of the wavefunction. Due to the parity selection rules, dipole transitions are only allowed between g and u states. In addition, the spin selection rule $\Delta S = 0$ holds, as the perturbed Hamiltonian is spin-independent. Thus, the only allowed transitions are $S_i^g \rightarrow S_j^u$ and $S_i^u \rightarrow S_j^g$ in both the linear and nonlinear

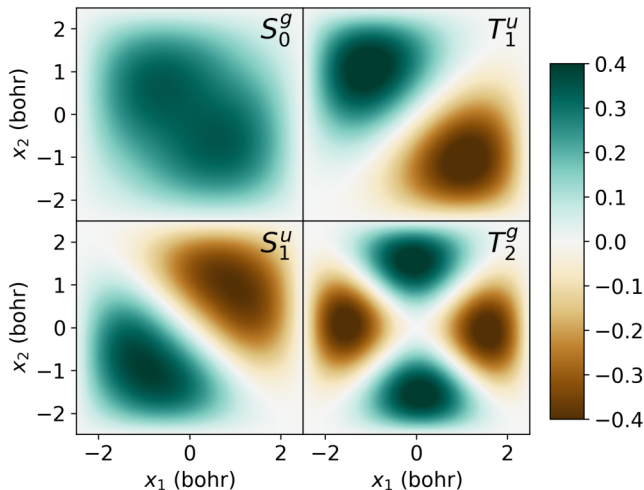


Figure 2: Top panel: Eigenstates depicted in the configuration space $x_1 - x_2$ (left) and eigenvalues (right) of the unperturbed system of two electrons in a 1D potential well of infinite depth (Eq. (14)). The states are labeled as $\mathcal{S}_i^{g/u}$, where \mathcal{S} indicates the spin state (singlet S or triplet T), i the order in energy within the spin channel, and g/u the parity with respect to inversion of the coordinates. Colorbar units are bohr^{-1} . Bottom panel: eigenvalues of the first five eigenvectors of the unperturbed Hamiltonian in Eq. (14).

regimes.

The linear and nonlinear absorption spectra of the 1DW obtained by applying an electric field impulse of $\kappa = 0.01 \text{ bohr}^{-1}$ and 0.80 bohr^{-1} , respectively, are shown in Fig. 3. Given the well length and the spacing of the ground-state eigenvalues, the field corresponding to $\kappa \leq 0.02 \text{ bohr}^{-1}$ can be considered weak. The resulting cross sections show an intrinsic broadening of 0.04 Ha due to the finite duration of the time propagation.

In the lower panel of Fig. 3 the linear spectrum shows a single maximum at 0.67 Ha , corresponding to the $S_0^g \rightarrow S_1^u$ transition. In contrast, the nonlinear absorption cross section features several peaks spread over the range $(0.4\text{--}1.4) \text{ Ha}$, namely at lower and

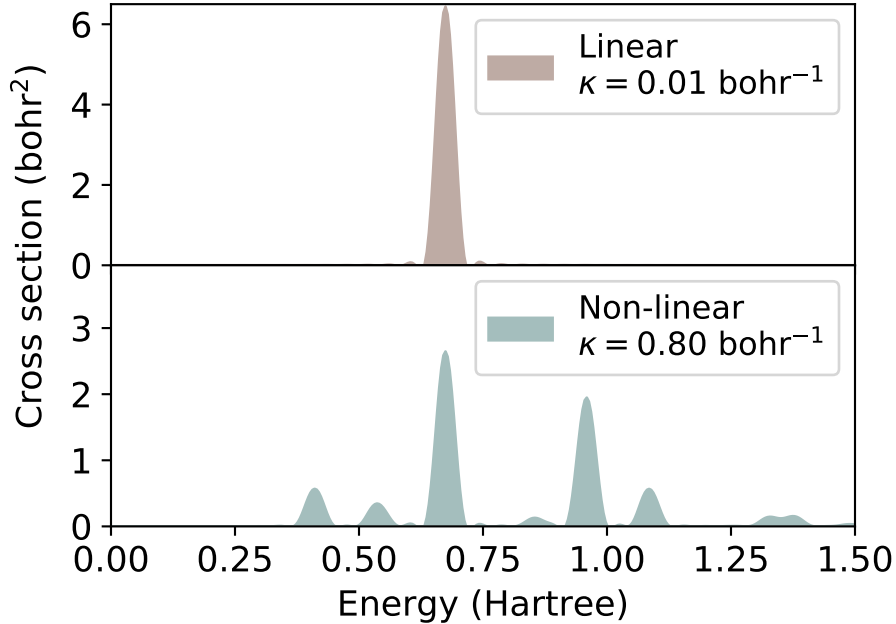


Figure 3: Comparison between the linear and nonlinear absorption spectra of a 1D square potential well containing two electrons (1DW). The linear absorption spectrum (upper panel) is obtained by applying an impulsive electric field with strength $\kappa = 0.01 \text{ bohr}^{-1}$ (weak field regime). The nonlinear absorption spectrum (lower panel) is obtained by applying an electric field with strength $\kappa = 0.80 \text{ bohr}^{-1}$ (strong field regime).

higher energies with respect to the excitation in the linear regime. In the nonlinear regime, the maximum corresponding to the $S_0^g \rightarrow S_1^u$ transition at 0.67 Ha is not suppressed but its spectral weight is approximately halved.

To analyze the transitions involved in the nonlinear cross section, in Fig. 4 we consider separately the contributions of three components, namely $\sigma_{S_0}(\omega)$, $\sigma_{S_1}(\omega)$, and $\sigma_{\{S_m\}}(\omega)$, with $m \geq 2$. The first and second components account for the absorption from the ground state and from the first excited state, while the third one includes the contributions from all higher excited states. These components are calculated from Eq. (6) evaluating the sums up to the first 100 eigenstates of \hat{H}_0 . Convergence is verified by the sum rule in Eq. (8). Dirac deltas in Eq. (6) are broadened in order to match the peak width of the cross sections obtained from the solution of the time-dependent

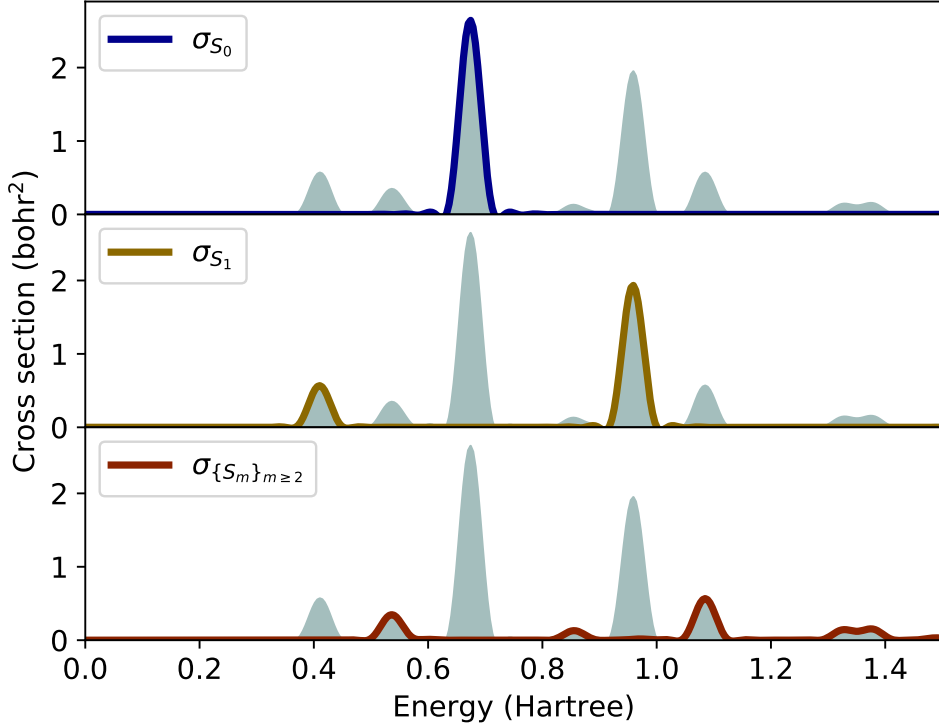


Figure 4: Nonlinear absorption cross section of the 1DW subject to a strong electric field impulse with $\kappa = 0.80 \text{ bohr}^{-1}$. The cross section is split into ground-state absorption (blue curve), first excited-state absorption (yellow curve) and absorption from higher excited states (red curve).

Schrödinger equations.

The component $\sigma_{S_0}(\omega)$ (top panel of Fig. 4) includes the same contribution as the linear cross section, $S_0^g \rightarrow S_1^u$ (see top panel of Fig. 3). Therefore the additional peaks in the lower panel of Fig. 3 result from ESA. In particular, the two peaks at 0.41 Ha and 0.96 Ha (see middle panel of Fig. 4) are due to the absorption from the first excited state (S_1^u) and involve the transitions to *gerade* excited states $S_1^u \rightarrow S_2^g$ and $S_1^u \rightarrow S_3^g$, respectively. Simply on the base of symmetry, the excited S_2^g and S_3^g cannot be reached from the ground state S_0^g . By inspecting the bottom panel of Fig. 4, we notice that the higher-order contributions to the absorption consist of a number of weak peaks below and above the maximum at 0.67 Ha. For example, the maximum at about 1.1 Ha corresponds to the transition $S_2^g \rightarrow S_4^u$.

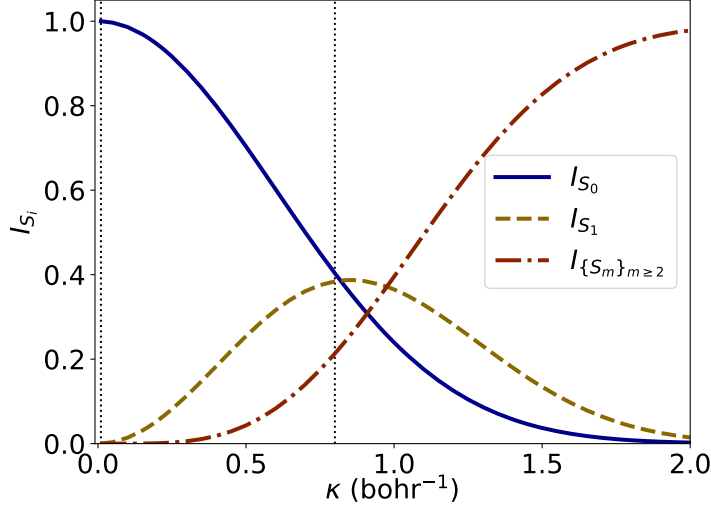


Figure 5: Normalized weights [see Eq. (17)] of the three components of the absorption cross section given in Figure 4 as a function of the strength of the electric field impulse κ . The dashed vertical bars correspond to the values of κ used in Figure 3.

To gain further understanding on the information provided by the non-perturbative approach presented so far, it is interesting to inspect the variation of the relative weights of ground-state and excited-state absorption as a function of the field strength. These contributions are quantified by

$$I_{S_i} = \frac{c}{4\pi^2} \int_0^{+\infty} d\omega \sigma_{S_i}(\omega) . \quad (17)$$

The values of I_{S_0} , I_{S_1} , and I_{S_m} , with $m \geq 2$, are shown in Fig. 5 as a function of κ . Note that each contribution refers to a specific subset of the absorption but they all include contributions *at all perturbation orders*. The solid curve in Fig. 5 represents the weight of the ground-state cross section I_{S_0} . For $\kappa \approx 0$, we have that $I_{S_0} \approx 1$, which confirms that there is only GSA in the linear regime, as expected. At increasing values of κ , I_{S_0} decreases monotonically: ESA becomes relevant as the response of the system deviates from linearity. For $\kappa > 1.44 \text{ bohr}^{-1}$, we have that $I_{S_0} < 0.05$, meaning that the GSA becomes negligible above this threshold. The dashed curve in Fig. 5

represents the weight of the first-excited-state cross section I_{S_1} . It vanishes for small κ , reaches its maximum at $\kappa = 0.85$ Ha, and decreases monotonically for higher values of κ . The dashed-dotted curve in Fig. 5 accounts for the weight of the higher-order absorption cross section $I_{\{S_m\}}$, where $m \geq 2$. Also $I_{\{S_m\}}$ does not contribute at small κ . It increases monotonically starting from $\kappa \approx 0.25$ bohr $^{-1}$ and reaches its saturation value, $I_{\{S_m\}} = 1$, for values of κ approaching 2 bohr $^{-1}$. In the strong field limit ($\kappa > 1.75$ bohr $^{-1}$), the only non-negligible component of the cross section is $I_{\{S_m\}}$.

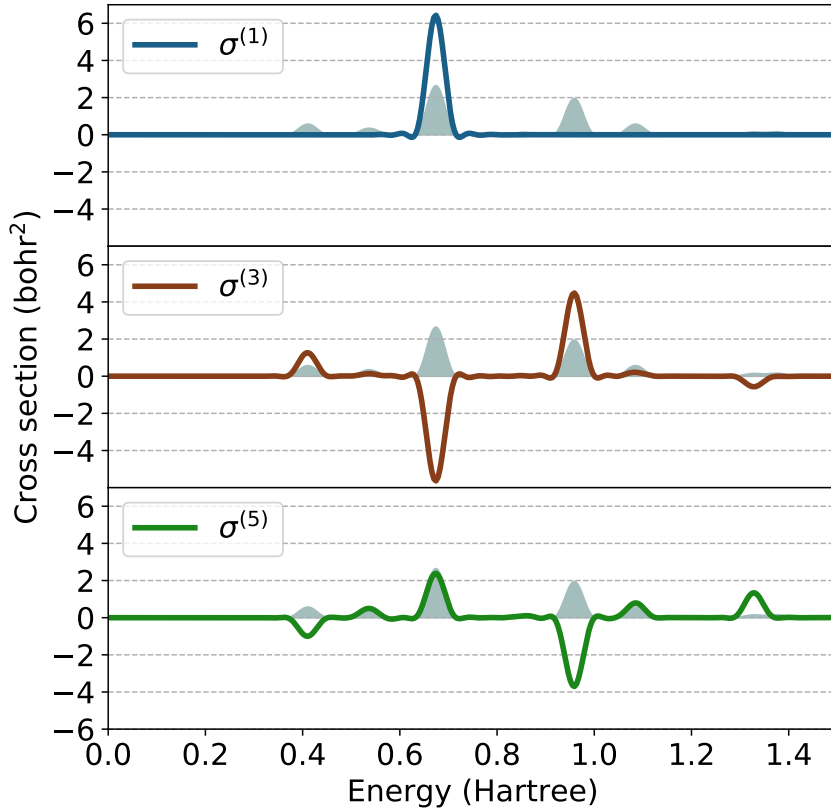


Figure 6: Perturbative components $\sigma^{(1)}$, $\sigma^{(3)}$ and $\sigma^{(5)}$ (Eqs. (7), (9) and (12) respectively) of the nonlinear absorption cross section the 1DW subject to the electric field impulse $\kappa = 0.80$ bohr $^{-1}$. For reference, the total cross section (Eq. 6), also shown in the bottom panel of Fig. 3, is plotted as shaded area in the background of each panel.

We complete our analysis by considering the perturbative expansion of the nonlinear absorption cross section, as discussed in Section 2. The perturbative terms $\sigma^{(1)}(\omega)$,

$\sigma^{(3)}(\omega)$, and $\sigma^{(5)}(\omega)$ are shown in Fig. 6. They are computed from Eq. (7), (9), and (12). The impulse cross section $\sigma(\omega)$ calculated with the impulse response method for $\kappa = 0.80 \text{ bohr}^{-1}$ is also shown for comparison.

The first-order cross section $\sigma^{(1)}(\omega)$ assumes only positive values and contributes only to the maximum at 0.67 Ha. The first nonlinear non-vanishing component of the cross section, which thus accounts for ESA processes, is the third-order one, $\sigma^{(3)}$, which assumes both positive and negative values. A pronounced peak with negative strength is found at 0.67 Ha and corresponds to the third-order correction of the ground-state transition $S_0^g \rightarrow S_1^u$. This term cancels out almost completely the contribution from $\sigma^{(1)}$ at the same energy. Maxima with positive intensities appear at about 0.4 Ha and 1.0 Ha.

However, $\sigma^{(3)}$ alone is not sufficient to describe the nonlinear excitations in the 1DW, as shown by comparing this term with the total impulse cross section (see Fig. 6, middle panel). For this reason, it is necessary to inspect also the contributions from the fifth-order cross section, namely $\sigma^{(5)}$. This term has maxima and minima at the same energy as those of $\sigma^{(3)}$ but with intensities of opposite sign. This is a general feature of perturbation theory. In particular, the peak at 0.67 Ha is positive and overlaps almost perfectly with the one in the impulse cross section shown in the background (see bottom panel of Fig. 6). Minima are found at approximately 0.4 Ha and 1.0 Ha, at the same energies where $\sigma^{(3)}$ exhibits maxima. The absolute values of the corresponding intensities are very similar, suggesting that these contributions should cancel out. But we could not fully reproduce the total cross section obtained via direct time propagation by means of the perturbative approach, not even adding contributions up to the seventh order.

4 Conclusions

In summary, we have examined the real-time propagation of a quantum system from its ground state induced by an instantaneous impulsive electrical field as a tool for

investigating computationally nonlinear optical properties of many-electron systems. By employing the resolution of the identity on a basis set of eigenvalues of the unperturbed Hamiltonian, we have analyzed the total cross section, calculated as an impulse response in terms of partitioned contributions originating from a different set of ground and excited-state transitions. In this way, we have determined the weight of each set as a function of the field strength. Comparing the impulse response cross section with the first few terms of the perturbative series in powers of the field strength, we have shown that the impulse response technique provides a compact description of nonlinear processes at all orders altogether, even in those cases where the convergence of the perturbative series is very slow. To assess the capabilities of the method itself independently of other approximations, we have adopted a one-dimensional toy system to numerically verify our findings using a finite-differences propagation scheme in real space and real time.

The approach examined in this work provides us with vital information about the whole spectrum at once. This is particularly relevant for investigating nonlinear systems, for which the total absorption cannot be decomposed into the sum of the individual absorption of monochromatic radiation for each frequency. Nonlinearities arising from nuclear motion can be straightforwardly included via hybridization with a scheme for the dynamics of the nuclei. The method, however, does not access the dependence of the spectrum on the pulse shape. Therefore, it cannot be applied to study processes such as two-photon absorption or ultrafast transients.

We conclude that the impulse response as computed in real time can profitably be employed to study properties in nonlinear dynamical systems. Specifically, we have shown that the impulsive method provides relevant information about the steady-state absorption of time-invariant systems in which the nonlinearity manifests itself as a mere dependence of the spectrum on the field strength. The method, as is, is therefore not suitable to investigate those cases in which hysteresis loops or other memory-dependent phenomena are important. For cases in which the interest in nonlinearities is not restricted to wave mixing at a predefined order, the computation of the nonlinear

impulsive response function from real-time propagation can outperform the ordinary approach based on perturbation theory to investigate phenomena driven by excited state absorption such as reverse saturable absorption, optical switching, and optical limiting.

Acknowledgement

A.G. acknowledges financial support from the German Academic Exchange Service (DAAD) and from HPC Europa 3. Computational resources provided by the North-German Supercomputing Alliance (HLRN), project bep00060, and by the High Performance Computing Center Stuttgart (HLRS).

Supporting Information Available

The following files are available free of charge. In Sec. S1 the general expression for the nonlinear absorption cross section is derived. In Sec. S2 the spectral resolution of the cross section is derived. In Sec. Ref. 38 is cited therein.

References

- (1) Franken, P. A.; Hill, A. E.; Peters, C. W.; Weinreich, G. Generation of Optical Harmonics. *Phys. Rev. Lett.* **1961**, *7*, 118–119.
- (2) Damm, T.; Kaschke, M.; Noack, F.; Wilhelmi, B. Compression of picosecond pulses from a solid-state laser using self-phase modulation in graded-index fibers. *Opt. Lett.* **1985**, *10*, 176–178.
- (3) Perry, M. D.; Mourou, G. Terawatt to Petawatt Subpicosecond Lasers. *Science* **1994**, *264*, 917–924.

- (4) Boyd, R. W. *Nonlinear Optics, Third Edition*, 3rd ed.; Academic Press, Inc.: USA, 2008.
- (5) Brabec, T.; Krausz, F. Intense few-cycle laser fields: Frontiers of nonlinear optics. *Rev. Mod. Phys.* **2000**, *72*, 545–591.
- (6) Lorin, E.; Lytova, M.; Memarian, A.; Bandrauk, A. D. Development of nonperturbative nonlinear optics models including effects of high order nonlinearities and of free electron plasma: Maxwell–Schrödinger equations coupled with evolution equations for polarization effects, and the SFA-like nonlinear optics model. *Journal of Physics A: Mathematical and Theoretical* **2015**, *48*, 105201.
- (7) Peterson, R. L. Formal Theory of Nonlinear Response. *Rev. Mod. Phys.* **1967**, *39*, 69–77.
- (8) Safi, I.; Joyez, P. Time-dependent theory of nonlinear response and current fluctuations. *Phys. Rev. B* **2011**, *84*, 205129.
- (9) Strelkov, V. V. High-order optical processes in intense laser field: Towards nonperturbative nonlinear optics. *Phys. Rev. A* **2016**, *93*, 053812.
- (10) Goings, J. J.; Lestrangle, P. J.; Li, X. Real-time time-dependent electronic structure theory. *Wiley Interdiscip. Rev. Comput. Mol. Sci.* **2018**, *8*, 1–19.
- (11) Ullrich, C. A. *Time-dependent density-functional theory: concepts and applications*; Oxford University Press: Oxford, 2011.
- (12) Marques, M. A.; Maitra, N. T.; Nogueira, F. M.; Gross, E. K. U.; Rubio, A. *Fundamentals of Time-Dependent Density Functional Theory*; Lecture Notes in Physics book series; Springer, Berlin, Heidelberg, 2012.
- (13) Takimoto, Y.; Vila, F. D.; Rehr, J. J. Real-time time-dependent density functional theory approach for frequency-dependent nonlinear optical response in photonic molecules. *J. Chem. Phys.* **2007**, *127*.

- (14) Attaccalite, C.; Grüning, M. Nonlinear optics from an *ab initio* approach by means of the dynamical Berry phase: Application to second- and third-harmonic generation in semiconductors. *Phys. Rev. B* **2013**, *88*, 1–10.
- (15) Uemoto, M.; Kuwabara, Y.; Sato, S. A.; Yabana, K. Nonlinear polarization evolution using time-dependent density functional theory. *J. Chem. Phys.* **2019**, *150*, 094101.
- (16) Luppi, E.; Head-Gordon, M. Computation of high-harmonic generation spectra of H₂ and N₂ in intense laser pulses using quantum chemistry methods and time-dependent density functional theory. *Molecular Physics* **2012**, *110*, 909–923.
- (17) Yamada, A.; Yabana, K. Multiscale time-dependent density functional theory for a unified description of ultrafast dynamics: Pulsed light, electron, and lattice motions in crystalline solids. *Phys. Rev. B* **2019**, *99*, 245103.
- (18) Alonso, J. L.; Andrade, X.; Echenique, P.; Falceto, F.; Prada-Gracia, D.; Rubio, A. Efficient Formalism for Large-Scale Ab Initio Molecular Dynamics based on Time-Dependent Density Functional Theory. *Physical Review Letters* **2008**, *101*, 096403.
- (19) Falke, S. M.; Rozzi, C. A.; Brida, D.; Maiuri, M.; Amato, M.; Sommer, E.; De Sio, A.; Rubio, A.; Cerullo, G.; Molinari, E.; Lienau, C. Coherent ultrafast charge transfer in an organic photovoltaic blend. *Science* **2014**, *344*, 1001–1005.
- (20) Pittalis, S.; Delgado, A.; Robin, J.; Freimuth, L.; Christoffers, J.; Lienau, C.; Rozzi, C. A. Charge Separation Dynamics and Opto-Electronic Properties of a Diaminoterephthalate-C₆₀ Dyad. *Advanced Functional Materials* **2015**, *25*, 2047–2053.
- (21) Rozzi, C. A.; Pittalis, S. *Handbook of Materials Modeling*; Springer International Publishing: Cham, 2018; pp 1–19.

- (22) Yuen-Zhou, J.; Tempel, D. G.; Rodríguez-Rosario, C. A.; Aspuru-Guzik, A. Time-Dependent Density Functional Theory for Open Quantum Systems with Unitary Propagation. *Phys. Rev. Lett.* **2010**, *104*, 043001.
- (23) Newcomb, R. W. Distributional impulse response theorems. *Proceedings of the IEEE* **1963**, *51*, 1157–1158.
- (24) Cocchi, C.; Prezzi, D.; Ruini, A.; Molinari, E.; Rozzi, C. A. *Ab initio* simulation of optical limiting: The case of metal-free phthalocyanine. *Phys. Rev. Lett.* **2014**, *112*, 1–5.
- (25) Dini, D.; Calvete, M. J.; Hanack, M. Nonlinear Optical Materials for the Smart Filtering of Optical Radiation. *Chem. Rev.* **2016**, *116*, 13043–13233.
- (26) Sun, Y.-P.; Riggs, J. E. Organic and inorganic optical limiting materials. From fullerenes to nanoparticles. *Int. Rev. Phys. Chem.* **1999**, *18*, 43–90.
- (27) Bellier, Q.; Makarov, N. S.; Bouit, P.-A.; Rigaut, S.; Kamada, K.; Feneyrou, P.; Berginc, G.; Maury, O.; Perry, J. W.; Andraud, C. Excited state absorption: a key phenomenon for the improvement of biphotonic based optical limiting at telecommunication wavelengths. *Phys. Chem. Chem. Phys.* **2012**, *14*, 15299–15307.
- (28) Fischer, S. A.; Cramer, C. J.; Govind, N. Excited-State Absorption from Real-Time Time-Dependent Density Functional Theory: Optical Limiting in Zinc Phthalocyanine. *The Journal of Physical Chemistry Letters* **2016**, *7*, 1387–1391.
- (29) Perfetto, E.; Stefanucci, G. Some exact properties of the nonequilibrium response function for transient photoabsorption. *Phys. Rev. A* **2015**, *91*, 033416.
- (30) Yabana, K.; Bertsch, G. F. Time-dependent local-density approximation in real time. *Phys. Rev. B* **1996**, *54*, 4484–4487.
- (31) Buckingham, A. D. Polarizability and hyperpolarizability. *Philos. Trans. R. Soc. London. Ser. A, Math. Phys. Sci.* **1979**, *293*, 239–248.

- (32) Santhi, A.; Namboodiri, V. V.; Radhakrishnan, P.; Nampoori, V. P. N. Spectral dependence of third order nonlinear optical susceptibility of zinc phthalocyanine. *J. Appl. Phys.* **2006**, *100*, 053109.
- (33) Marian, C. M. Spin-orbit coupling and intersystem crossing in molecules. *Wiley Interdiscip. Rev. Comput. Mol. Sci.* **2012**, *2*, 187–203.
- (34) Oliveira, M. J. T.; Castro, A.; Marques, M. A. L.; Rubio, A. On the Use of Neumann’s Principle for the Calculation of the Polarizability Tensor of Nanostructures. *Journal of Nanoscience and Nanotechnology* **2008**, *8*, 3392–3398.
- (35) Su, Q.; Eberly, J. H. Model atom for multiphoton physics. *Phys. Rev. A* **1991**, *44*, 5997–6008.
- (36) Tancogne-Dejean, N.; Oliveira, M. J. T.; Andrade, X.; Appel, H.; Borca, C. H.; Le Breton, G.; Buchholz, F.; Castro, A.; Corni, S.; Correa, A. A.; De Giovannini, U.; Delgado, A.; Eich, F. G.; Flick, J.; Gil, G.; Gomez, A.; Helbig, N.; Hübener, H.; Jestädt, R.; Jornet-Somoza, J.; Larsen, A. H.; Lebedeva, I. V.; Lüders, M.; Marques, M. A. L.; Ohlmann, S. T.; Pipolo, S.; Rampp, M.; Rozzi, C. A.; Strubbe, D. A.; Sato, S. A.; Schäfer, C.; Theophilou, I.; Welden, A.; Rubio, A. Octopus, a computational framework for exploring light-driven phenomena and quantum dynamics in extended and finite systems. *The Journal of Chemical Physics* **2020**, *152*, 124119.
- (37) The simulations were performed on a regular spatial grid with a spacing of 0.015 bohr and $L = 5.0$ bohr. The dipole impulsive perturbation is $\hat{H}'(t) = -\hat{d}\kappa\delta(t)$, where $\hat{d} = \hat{x}_1 + \hat{x}_2$. After the impulse is applied, the wavefunction is propagated up to 150 Ha^{-1} , employing a time step of 0.002 Ha^{-1} .
- (38) Jackson, J. D. *Classical electrodynamics*, 3rd ed.; Wiley: New York, NY, 1999.

Graphical TOC Entry

